Modeling Thermochemical Solar-to-Fuel Conversion: CALPHAD for Thermodynamic Assessment Studies of Perovskites, Exemplified for (La,Sr)MnO_3

*Alexander H. Bork, Erwin Povoden-Karadeniz, and Jennifer L. M. Rupp**

Two-step solar thermochemical fuel production has the potential to reduce global greenhouse gas emissions and replace fossil fuels. The success of the technology relies on the development of materials with high thermochemical efficiency. Perovskites with the general structure ABO_3 have received much attention recently due to impressive fuel productivity and their amenability of substituting and doping both A- and B-site. Despite the potential of perovskites for solar-to-fuel conversion, literature on their solar thermochemical efficiency is scarce and finding the best chemical composition and optimum operation conditions is unknown. For this purpose, this study suggests to use Computer Coupling of Phase Diagrams and Thermochemistry (CALPHAD) data libraries to access the relevant thermodynamic properties of perovskites. This work demonstrates the usefulness of employing CALPHAD data by a full thermodynamic study of the model case compositions of $La_{1-x}Sr_xMnO_{3-\delta}$. This study uses data on oxygen-nonstoichiometry and heat capacity in the temperature range of 1073–1873 K relevant for solar-to-fuel. Unlike earlier thermodynamic assessments of perovskites that rely on a single literature source and a limited temperature range, the CALPHAD approach takes all available data in literature into consideration. Thermochemical equilibrium models of fuel yields are accompanied by validations toward experimental results in literature, and this study highlights the effects of strontium doping level on the efficiency.

1. Introduction

Two-step thermochemical solar-to-fuel production is an efficient way to store intermittent solar energy in renewable fuels, and it has the potential to reduce dependence on fossil fuels in the future.[1,2] In the thermochemical two-step cycle a metal oxide utilizes solar thermal energy to catalyze the production of syngas (H_2 and CO), so-called solar-fuel, from water and CO_2. Recently perovskites have received much attention due to impressive fuel productivity for solar-to-fuel conversion processes.[3–6] For those materials, the thermochemical reaction can be exemplified through the oxygen nonstoichiometry changes of the perovskite with the general structure ABO_3, whereby its reduction in a reactor is carried out in a first high-temperature step

$$ABO_3 \leftrightarrow ABO_{3-\delta} + \frac{\delta}{2} O_2(g) \tag{1}$$

In a second step, the perovskite is reoxidized during exposure to H_2O and CO_2

$$ABO_{3-\delta} + \delta H_2O \leftrightarrow ABO_3 + \delta H_2(g) \tag{2a}$$

$$ABO_{3-\delta} + \delta CO_2 \leftrightarrow ABO_3 + \delta CO(g) \tag{2b}$$

For the first and second step, temperatures are typically 1000 and 1500 °C respectively, see **Table 1**. The efforts in material development for solar-to-fuel conversion have been directed at fabrication of ceramics with high fuel yield during solar-thermochemical cycling. However, the thermochemical efficiency, defined as the chemical energy of the produced fuel divided by the solar thermal energy input is a more suitable parameter for comparison of material performance.[7–10] Despite the promise of recently suggested perovskites, the most investigated material in terms of solar thermochemical efficiency is ceria. Ceria solids provide fast oxidation rates during fuel production and chemical stability at high temperatures[11,12] and in CO_2 environment.[13] It is a well-investigated material with decades of thermochemical studies[14,15] and knowledge from fuel cell and electrolyzers,[16–18] or three-way catalysts;[19,20] still the actual solar thermochemical efficiency is debated. This is obvious if we consider that, the calculated solar-to-fuel conversion efficiencies vary from 19% to 40% in Table 1, from Refs. [9,21–23]. The discrepancy for ceria arises in part because different literature sources[14,24,25] are used for the same material, but also because different assumptions are made on the reactor, e.g., heat recovery and vacuum pump efficiency. It emphasizes the

A. H. Bork, Prof. J. L. M. Rupp
Electrochemical Materials
Department of Materials
ETH Zurich
Zurich CH-8093, Switzerland
E-mail: jennifer.rupp@mat.ethz.ch

Dr. E. Povoden-Karadeniz
Institute of Materials Science and Technology
TU Wien
Vienna AT-1060, Austria

DOI: 10.1002/aenm.201601086

Table 1. Comparison of efficiency and equilibrium hydrogen fuel yields per mole oxide for strontium doped lanthanum manganites and ceria in literature. First column shows the material composition, followed by the reference for the reported hydrogen yield and efficiency. The temperature range of the two-step cycle and oxygen partial pressure during reduction is shown for the respective analysis (T_{ox}–T_{red}). In some of the studies highlighted above, Refs. [9,21–23], the predictions are based on data found in literature indicated by the column "Input Data" and the measured temperature range for this input data is shown in the column "$T_{\text{Input data}}$".

Material	Ref.	η_{solar} [%]	n_{H2} [moles]	T_{ox}–T_{red} [K]	pO_2 [atm]	$T_{\text{Input data}}$ [K]	Input data
$La_{0.7}Sr_{0.3}MnO_3$	[9]	17	0.11	1000–1800	10^{-5}	873–1273	[26]
$La_{0.6}Sr_{0.4}MnO_3$	[9]	15	0.09	1000–1800	10^{-5}	873–1273	[26]
$La_{0.7}Sr_{0.3}MnO_3$	[27]	NA	0.058	1073–1673	10^{-5}	1073–1673	[26,27]
$La_{0.6}Sr_{0.4}MnO_3$	[27]	NA	0.095	1073–1673	10^{-5}	1073–1673	[26,27]
$La_{0.6}Sr_{0.4}MnO_3$	[7]	NA	0.041	1200–1673	10^{-4}	1573–1773	
$La_{0.6}Ca_{0.4}MnO_3$	[7]	NA	0.053	1200–1673	10^{-4}	1573–1773	
$La_{0.6}Sr_{0.4}Mn_{0.6}Al_{0.4}O_3$	[7]	NA	0.061	1200–1673	10^{-4}	1573–1773	
$La_{0.6}Ca_{0.4}Mn_{0.6}Al_{0.4}O_3$	[7]	NA	0.066	1200–1673	10^{-4}	1573–1773	
$La_{0.6}Sr_{0.4}MnO_3$	This work	12	0.07	1000–1800	10^{-6}	1073–1873	[28]
$La_{0.7}Sr_{0.3}MnO_3$	This work	19	0.055	1473–1773	10^{-6}	1073–1873	[28]
$La_{0.8}Sr_{0.2}MnO_3$	This work	21	0.01	1773–1773	10^{-6}	1073–1873	[28]
CeO_2	[22]	40	NA	1373–1773	10^{-5}	1023–1773	[24]
CeO_2	[21]	29	NA	1373–1773	10^{-5}	909–1773	[14]
CeO_2	[23]	19	NA	1373–1773	10^{-5}	1023–1273	[25]

importance of establishing reliable input data as well as to take particular note of the assumptions when different studies are compared.[8,23]

Focusing on the recently suggested material class of perovskites, one key advantage is the amenability of their ABO_3 crystal structure for doping on both of the A- and B-cationic sites, which offers wide possibilities to inflict significant changes in the oxygen nonstoichiometry and also on their thermodynamic properties when compared to the state-of-the-art material ceria for solar-to-fuel.[5,19,26,29] As prominent as the potential of novel perovskites compounds may be, literature on their thermodynamic properties and efficiency calculations for the field of solar-to-fuel conversion is scarce. In order to suggest the best materials toward a high thermochemical efficiency, smart approaches in computation and modeling are required to assess the performance of the vast compositional space of perovskites for solar-to-fuel conversion. Earlier thermochemical studies of perovskites and predictions of their solar-to-fuel performance rely on a single literature source,[9,27] or data that does not cover the entire technological relevant temperature range.[7] To establish reliable estimates of the actual efficiency there is a great need to map accurate thermodynamic properties of perovskites versus the effective operation conditions (e.g., temperature range, chemistry of dopants).

In this work, we employ Computer Coupling of Phase Diagrams and Thermochemistry (CALPHAD)[30] data as input to evaluate the material class of perovskites for the first time in solar-to-fuel conversion technology. There are three major advantages of using data from CALPHAD libraries for thermodynamic assessments toward solar-to-fuel. First, it is statistically more accurate because it does not rely on a single measurement, as previous studies on perovskites, but the evaluated perovskite thermodynamics represents the best fit to all existing experimental data in the literature on oxygen nonstoichiometry, phase changes, heat capacity, enthalpy, and Gibbs energy of formation. Secondly, all relevant data is given in the entire technologically relevant temperature range of 1073–1873 K developed in accordance with Refs. [31,28,32–34]. Thirdly, CALPHAD enables the description of multicomponent systems on a physicochemical base, which is of great advantage for evaluation of perovskites due to the innumerable possible compositions in solid solutions. We refer the reader to a general introduction to CALPHAD Ref. [30]. The concept of the approach in this work is shown in the **Figure 1**, illustrating how CALPHAD data on oxygen nonstoichiometry and heat capacity is used as input. From this input, we derive thermodynamic functions and calculate the equilibrium fuel yields and thermochemical efficiency. Specifically, we have selected $La_{0.6}Sr_{0.4}MnO_{3-\delta}$, $La_{0.7}Sr_{0.3}MnO_{3-\delta}$, and $La_{0.8}Sr_{0.2}MnO_{3-\delta}$ as model systems and compare our CALPHAD based results to experimental results in literature by Yang et al.[27] and Scheffe et al.[9]

Through this work, the benefits of using CALPHAD are demonstrated on A-site doping in lanthanum manganite perovskites, but importantly, the approach can easily be extended to other B-site doped perovskites to implicate predictions of new efficient materials in the future. Developing and expanding the knowledge of the oxygen nonstoichiometry and thermodynamic properties of the perovskite material class is equally relevant in other energy research areas where those parameters determine the material performance, e.g., thermal energy storage materials,[36,37] chemical looping combustion,[38,39] and metal oxides generating either syngas or methane.[40]

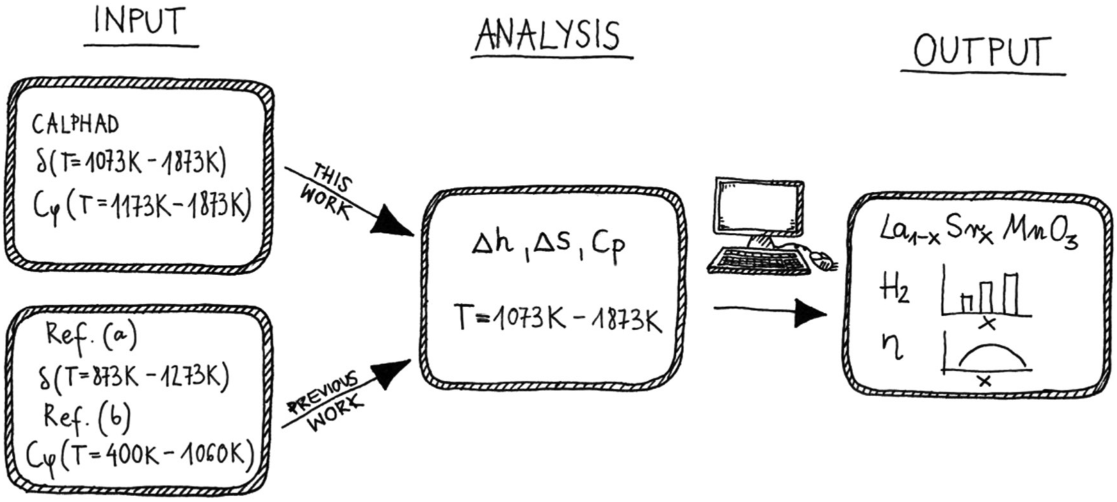

Figure 1. Overview of approach illustrating that different data sets are used as input for the calculations in this work compared to previous work.[9,27] Input of those calculations are based on Ref. a): Tagawa et al.[26] and Ref. b): Jacob and Attaluri.[35] As input for this work, we use CALPHAD data of oxygen nonstoichiometry in the temperature range 1073–1873 K and heat capacity in the range 1173–1873 K. The input data of oxygen nonstoichiometry data are analyzed and the thermodynamic functions of partial molar enthalpy and entropy can be derived, and heat capacity is extrapolated to the temperature range 1073–1873 K. The thermodynamic functions are used further to predict equilibrium hydrogen fuel yields (n_{H_2}) and the thermochemical solar-to-fuel efficiency (η_{solar}) in the technologically relevant temperature range of 1073–1873 K for solar-to-fuel.

2. Motivation and Advantages of CALPHAD Modeling of Strontium-Doped Lanthanum Manganite

In solar-to-fuel conversion, the oxygen nonstoichiometry of a metal oxide at a given temperature and oxygen partial pressure determines the amount of fuel that can be produced in each thermochemical cycle and is therefore a crucial parameter for modeling conversion efficiency. Strontium-doped lanthanum manganite perovskites have shown a high potential for solar-to-fuel due to a considerable oxygen nonstoichiometry and desirably high fuel yields and is therefore an interesting candidate for this analysis.[6,9,27,7,41] Two notable assessments of strontium-doped lanthanum manganites for solar-to-fuel conversion[9,27] rely, in their predictions, on extrapolations of oxygen nonstoichiometry based on the thermogravimetric experiments by Tagawa et al.[26] originally assessed for the solid oxide fuel cell application in the temperature range of 873–1273 K. Based on these experimental input data, Scheffe et al.[9] applies a defect model involving reduction of tetravalent manganese to trivalent manganese with the addition of a defect-cluster model for higher oxygen nonstoichiometries. Yang et al.[27] bypasses interpretation of the defect behavior; instead, they extrapolate oxygen nonstoichiometry from knowledge of the enthalpy and entropy for oxygen vacancy formation. With the assumption that these thermodynamic functions are temperature independent, they are able to extrapolate the nonstoichiometry to higher temperatures through an iterative approach. No doubt, both models are useful in extrapolating to the technologically relevant and higher temperature range of 1073–1873 K. Nevertheless, discrepancies between measured data and predictions are anticipated at temperature ranges where measurements are not provided as experimental input data due to the mismatch in temperature ranges. As an alternative and for the purpose of characterizing the oxygen nonstoichiometry in the system $La_{1-x}Sr_xMnO_{3-\delta}$ over a wider temperature range, we use now a CALPHAD database given in the entire and relevant temperature range of 1073–1873 K compiled by Povoden–Karadeniz et al.,[34] which contains the CALPHAD modeling of defect chemistry developed by Grundy et al.[32]

In essence, the CALPHAD solution phase model of $La_{1-x}Sr_xMnO_3$[28] is based on the combination of previous CALPHAD optimizations of the systems La-Mn-O,[31] Sr-Mn-O,[42] and La-Sr-O.[43] In the CALPHAD computational assessment technique, the thermodynamic description of a complex solution phase, such as $La_{1-x}Sr_xMnO_3$ is based on a combination of molar Gibbs energies of the pure forming compounds of the phase (compound energy formalism). In the case of $La_{1-x}Sr_xMnO_3$, these are La_2O_3SrO, $LaMnO_3$, and $SrMnO_3$. In addition, the thermodynamic properties of the given phases, i.e., enthalpies of mixing, Gibbs energies, and chemical potentials, the observed phase equilibria, i.e., competing phase stabilities in all subsystems are considered in the model parameterizations. Hence, all thermodynamic and phase diagram data of a phase are simultaneously and consistently reproduced, and by combining the assessments of these ternary systems it is possible to extrapolate physicochemically properly to the quaternary La-Sr-Mn-O system. For modeling and parameter optimization details, the reader is referred to the CALPHAD assessment.[28,44] Grundy et al.[28] demonstrated that the compound energy formalism, which allows for the computational definition of thermodynamics of complex solution phases in accordance with its crystal structural site occupancies, can be used for modeling defect chemistry. The key for this modeling technique is the correct CALPHAD formulation of the Gibbs energy surface spanning the oxidized and reduced compounds

Table 2. Overview of type of experiments taken into consideration for development of the CALPHAD model of $La_{1-x}Sr_xMnO_3$, for details and references for each experiment, the reader is referred to the work by Grundy et al.[28,44]

Property	Varied conditions	Experiment
	La-Mn-O compound	
Phase equilibria	T, pO_2	Isothermal heat treatment
Gibbs energy of formation	T, Oxygen content	Electromotive force
Enthalpy of formation	T, air	Calorimetry
Oxygen content	T, pO_2	Thermogravimetry
Mean Mn-valency	T, pO_2	Coulometric titration and iodometry
Oxygen sites (interstitial)	Standard conditions	Neutron diffraction
Vacancy sites (A, B)	pO_2	Neutron diffraction
Defect mechanism	pO_2	Electrical conductivity
	Sr-Mn-O compound	
Phase equilibria	T, pO_2	Isothermal heat treatment
Phase transformations	T, pO_2	Differential thermal analysis
Gibbs energy of decomposition	T, pO_2	Electromotive force
Oxygen content	T, pO_2	Thermogravimetry
	La-Sr-Mn-O perovskite	
Single-phase equilibrium in air	T, pO_2, composition	Isothermal heat treatment
Perovskite decomposition	T, pO_2, composition	Heat treatment
Enthalpy of formation	Composition	High-temperature reaction calorimetry
Gibbs energy of formation	T, composition	Electromotive force
Gibbs energy of formation, $La_{0.8}Sr_{0.2}MnO_3$	Constant T (1373 K)	Electromotive force
Oxygen content	T, pO_2	Thermogravimetry
Mean Mn-valency	Constant T (973 K), air	X-ray absorption spectroscopy

of a defect phase such as $La_{1-x}Sr_xMnO_3$ perovskite. The Gibbs energy of the phase, containing main defects and crystallographic site occupancies, $(La^{3+},Sr^{2+},Va)(Mn^{2+},Mn^{3+},Mn^{4+},Va)(O^{2-},Va)_3$, is given as a mixture of real and hypothetic "end-member" compounds, obtained by recombination of A-site cations, B-site cations, and oxygen or vacancies (Va). This description was optimized and validated further toward for example thermogravimetric data or calorimetric measurements in literature of $La_{1-x}Sr_xMnO_3$. Accepting further constraints in the modeling, such as reciprocal relations among compound energies, optimization of model parameters of neutral compounds by various types of experimental data on perovskite stability, average manganese valence, and oxygen nonstoichiometry, among others, delivers correct defect concentration as function of temperature and oxygen partial pressure in the relevant operation range of solar-to-fuel. **Table 2** lists all types of experiments that have been included in the parameter optimization of the perovskite phase. With CALPHAD-optimized compound Gibbs energy functions, the extension beyond the experimental thermal and partial pressure conditions is put on a physicochemical base. In the modeling, defect evolution as function of temperature and oxygen partial pressure is a consequence of the chosen crystal sublattice description and associated site occupancies, and the demand of least squares of errors between all experimental perovskite data listed in Table 2 and computed results. This is reasonable, as revealed in the good reproduction of all experimental data of oxygen nonstoichiometry from low to high temperatures, shown in Figure S2 in the Supporting Information.

Analyzing and assessing a new metal oxide (Me-O) can thus be used to extend this model system to even higher order multicomponent oxides, e.g., La-Sr-Mn-Me-O. Subsequently, it is possible to vary concentrations of all four metals (La, Sr, Mn, Me) and study the behavior of numerous new perovskite compositions toward solar-to-fuel or other technologies where thermodynamic properties determine the performance.

2.1. Comparison of CALPHAD Oxygen Nonstoichiometry to Experimental Input Data from Thermogravimetry Measurements and Extrapolations of Defect Chemistry

Here, we consider the oxygen nonstoichiometry of $La_{0.6}Sr_{0.4}MnO_{3-\delta}$ versus oxygen partial pressure derived from CALPHAD data libraries in the temperature range 1073–1873 K. It is compared to the experimental data of the thermogravimetric measurements by Tagawa et al.[26] at the temperatures of 1073 and 1273 K and by Takacs et al.[7] at the temperature 1573 K. See Figure S1 in the Supporting information for comparison of thermogravimetric measurements[26,7] and CALPHAD data only. Importantly, we highlight differences between CALPHAD oxygen nonstoichiometry and the values extrapolated from Tagawa's data toward higher temperature of 1573 and 1873 K.[9,27] For solar-to-fuel reactor operation, the whole temperature range from 1073 to 1873 K is significant. In **Figure 2**, the following observations can be made comparing the four data sets to the CALPHAD data set for the material $La_{0.6}Sr_{0.4}MnO_{3-\delta}$: The CALPHAD description reproduces the thermogravimetric data from Tagawa et al.[26] well in the original measurement range of 1073–1273 K, although small deviations are observed at a high value of nonstoichiometry. For example, at the 1273 K isotherm and a nonstoichiometry of $\delta = 0.2$, we observe a deviation of 0.8 in the logarithm of oxygen partial pressure between the two data sets. Likewise, the CALPHAD description reproduces the experimental oxygen nonstoichiometry data measured by Takacs et al.[7] in the temperature range 1573–1773 K, with a maximum difference of 0.4 in the logarithmic oxygen partial pressure, Figure 2 and Figure S1 in the Supporting Information. If one compares the experimental results between two different thermogravimetric analysis one can expect deviations of this size, due to sample preparation (e.g., particle size) and experimental setup (e.g., difficulties in controlling pO_2). Herein lies the advantage of CALPHAD; it is best fit to all existing data from different measurements[28] and higher statistical accuracy can be expected.

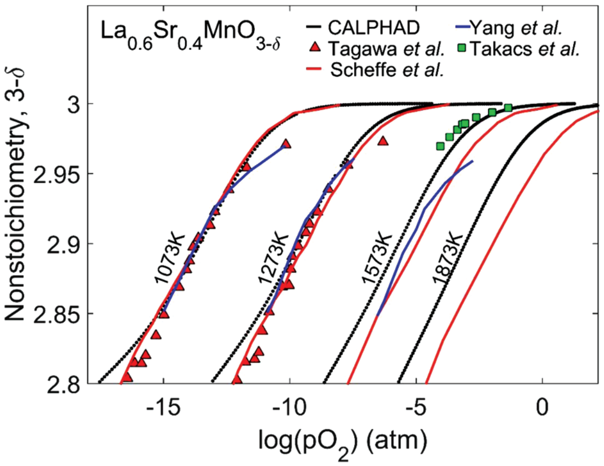

Figure 2. Oxygen nonstoichiometry of $La_{0.6}Sr_{0.4}MnO_{3-\delta}$ as a function of logarithmic oxygen partial pressure at a temperature of 1073, 1273, 1573, and 1873 K. Black dots are data extracted from CALPHAD descriptions of defect chemistry, red triangles represent experimental thermogravimetric data extracted from Tagawa et al.,[26] blue solid lines are model results data from Yang et al.,[27] solid red lines are model predictions from Scheffe et al.,[9] and green squares represent data from thermogravimetric measurements replotted from Takacs et al.[7]

Secondly, we observe that extrapolations made in both Yang's[27] and Scheffe's[9] study reproduce the data from Tagawa for the isotherms of 1073 and 1273 K very well. However, turning to higher temperatures, the extrapolations display discrepancies: At an exemplary oxygen partial pressure of 10^{-5} atm and a temperature of 1573 K, the oxygen nonstoichiometry is 0.075 in the CALPHAD description, whereas it is 0.09 and 0.1 corresponding to an overestimate of 17% and 33% in Yang's and Scheffe's description respectively. Consequently, extrapolation of results measured at lower temperatures leads to errors that increase in size for extrapolations over a wider temperature window.

After careful analysis of different literature sources, it is clear that the choice of data set is significant for the value of oxygen nonstoichiometry. Earlier studies, where extrapolations are made from thermogravimetric measurements in the temperature range 873–1273 K up to the relevant temperature range of 1073–1873 K display a discrepancy of 17%–33% in oxygen nonstoichiometry compared to the CALPHAD description. The solar-fuel that can be produced in each thermochemical cycle is proportional to the oxygen-nonstoichiometry. Thus, if the material would be fully reoxidized the solar-fuel production would, in the worst case, be overestimated by a value of up to 33%. CALPHAD libraries provide data in the relevant temperature range for solar-to-fuel operation of the selected perovskite example of $La_{0.6}Sr_{0.4}MnO_{3-\delta}$, with a high statistic accuracy, which is necessary to determine the thermochemical fuel production and efficiency with high reliability.

2.2. Oxygen Nonstoichiometry of $La_{1-x}Sr_xMnO_{3-\delta}$ Extracted from CALPHAD data Libraries for the Solar-to-fuel Temperature Range

In **Figure 3**, we describe the oxygen nonstoichiometry of the three compositions $La_{0.8}Sr_{0.2}MnO_{3-\delta}$, $La_{0.7}Sr_{0.3}MnO_{3-\delta}$, and $La_{0.6}Sr_{0.4}MnO_{3-\delta}$ as function of the logarithmic oxygen partial pressure. For this, the oxygen nonstoichiometry is extracted from CALPHAD libraries and is depicted over an unusually wide temperature window of 1073–1873 K for computations in the field. Analyzing the computed values, we confirm an increased oxygen release for higher temperatures and lower oxygen partial pressure for all tested compositions, Figure 3a–c. Consider for example the composition $La_{0.8}Sr_{0.2}MnO_{3-\delta}$, Figure 3a, the oxygen nonstoichiometry increases from 0.01 to 0.09, when the temperature is increased from 1373 to 1773 K at an oxygen partial pressure of 10^{-6} atm. Under practical solar-to-fuel operation, reduction is typically carried out at an oxygen partial pressure of 10^{-6} atm and a temperature of 1773 K.[1,11] For these conditions the oxygen nonstoichiometry is $\delta = 0.13$ for the composition $La_{0.7}Sr_{0.3}MnO_{3-\delta}$ (Figure 3b), while it is increased to $\delta = 0.18$ for the composition with increased strontium content of $La_{0.6}Sr_{0.4}MnO_{3-\delta}$ (Figure 3c). In Figure 3d the effect of strontium content is summarized at a temperature of 1773 K. Here, the substitution of Sr^{2+} on La^{3+} lattice sites results in a change in the oxidation state of the manganese cation from Mn^{3+} to Mn^{4+}, to maintain charge neutrality. The CALPHAD perovskite model for Sr^{2+}-doped lanthanum manganite considers competing oxygen vacancy formation and manganese charge disproportionation.[28]

Based on CALPHAD data we have shown the effect of strontium content on oxygen nonstoichiometry over a wide temperature of 1073–1873 K used for calculations of thermochemical efficiency for solar-to-fuel. In the following, we describe how the oxygen nonstoichiometry as function temperature and oxygen partial pressure can be used to extract the thermodynamic functions enthalpy and entropy for the reduction step in the solar to fuel conversion. These functions are necessary for the analysis of fuel yields with respect to the perovskite A-site doping chemistry in this work.

3. Thermodynamics of Perovskite-Type Oxides for Solar-to-fuel

The partial molar enthalpy (Δh_O) and entropy (Δs_O) of reduction for the perovskite are important for solar-to-fuel because they determine the driving force for converting H_2O and CO_2 into H_2 and CO. In accordance to Panlener et al.[24] the thermodynamic energies are related to oxygen partial pressure and temperature by the following relation

$$\frac{1}{2}RT\ln p_{O_2} = \Delta h_O - T\Delta s_O \tag{3}$$

where p_{O_2} is the oxygen partial pressure, R is the universal gas constant and T is temperature. For constant oxygen nonstoichiometry, δ, Equation (3) can be rearranged accordingly to

$$\frac{1}{2}\ln p_{O_2}\bigg|_{\delta=\text{constant}} = \frac{\Delta h_O}{RT} - \frac{\Delta s_O}{R} \tag{4}$$

Thus, Δh_O and Δs_O can be determined through an Arrhenius plot for sets of temperature T and $\ln pO_2$, where the slope of the straight line provides the enthalpy and the intercept gives the

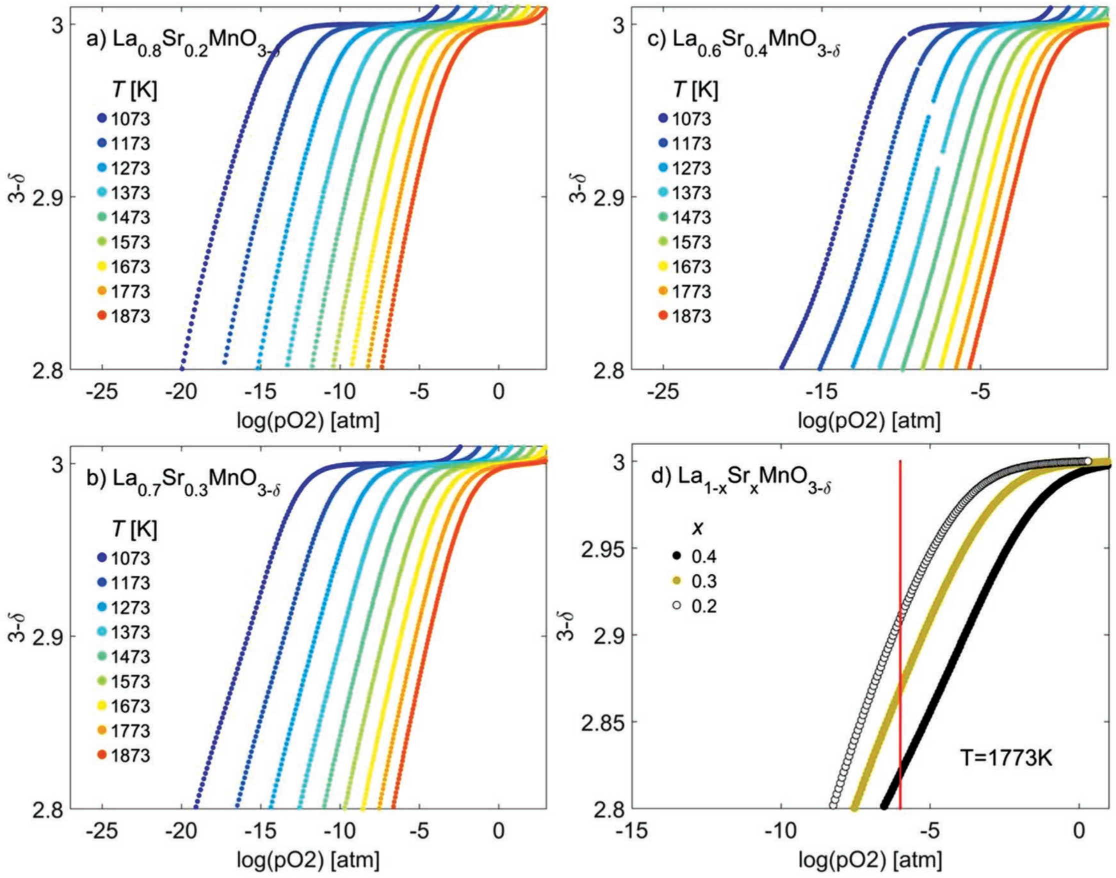

Figure 3. Oxygen nonstoichiometry plotted versus oxygen partial pressure for different temperatures in a window of 1073–1873 K extracted from CALPHAD libraries of defect chemistry for the compositions: a) $La_{0.8}Sr_{0.2}MnO_{3-\delta}$, b) $La_{0.7}Sr_{0.3}MnO_{3-\delta}$, and c) $La_{0.6}Sr_{0.4}MnO_{3-\delta}$. The effect of strontium content in $La_{1-x}Sr_{x}MnO_{3-\delta}$ is illustrated at a temperature of 1773 K in d), where the red line marks an oxygen partial pressure value of 10^{-6} atm.

entropy. The Gibbs free energy change of oxidation at any given oxygen nonstoichiometry, Δg_O, is calculated from enthalpy and entropy as function of temperature.

3.1. Comparison of Thermodynamics of $La_{0.6}Sr_{0.4}MnO_{3-\delta}$ Derived from CALPHAD Oxygen Nonstoichiometry to Experimental Thermogravimetric Data

Here, we select $La_{0.6}Sr_{0.4}MnO_{3-\delta}$ to evaluate partial molar enthalpy and entropy via Equation (4). Our CALPHAD oxygen nonstoichiometry based result is compared to the enthalpy and entropy, used in Ref.[9,27], based on thermogravimetric measurements by Tagawa et al.[26] **Figure 4**.

In Figure 4a we observe that based on the CALPHAD data, the enthalpy increases from 250 to 290 kJ mol^{-1} when the oxygen nonstoichiometry is increased from 0 to 0.2. In contrast, the enthalpy has a nearly constant value of 290 kJ mol^{-1} when calculated based on the data extracted from Tagawa's thermogravimetric measurement. Entropy is plotted versus oxygen nonstoichiometry in the range of 0–0.2 per mole metal oxide for the $La_{0.6}Sr_{0.4}MnO_{3-\delta}$ perovskite in Figure 4b. In accordance with the discrepancies observed for enthalpy, we observe a difference in the entropy between the two data sets. Namely, the entropy derived from the CALPHAD data decreases with reduction extent from 140 to 100 J mol^{-1} K^{-1} in the oxygen nonstoichiometry range of 0–0.2. The referred data also shows a decreasing entropy, but with a higher absolute value and steeper slope, from 180 to 110 J mol^{-1} K^{-1}.

Here it is noted that the CALPHAD result is derived from consideration of all available thermodynamic and phase stability data in the relevant temperature range of 1073–1873 K for optimization of model parameters. Importantly, the CALPHAD descriptions of defect formation are based on both measurements of oxygen nonstoichiometry (e.g., thermogravimetric analysis) and enthalpies measured directly by calorimetry,[45,46] resulting in a reliable description of the materials' thermodynamic properties for the temperature range targeted for solar-to-fuel applications. Having established the thermodynamic properties of the exemplary perovskite composition $La_{0.6}Sr_{0.4}MnO_{3-\delta}$ we now focus on the effect of different strontium contents on these properties.

3.2. Partial Molar Enthalpy and Entropy of the Perovskite Oxide $La_{1-x}Sr_{x}MnO_{3-\delta}$ Derived from CALPHAD Oxygen Nonstoichiometry

In the following, we ascertain the changes in thermodynamic properties as function of strontium doping, for

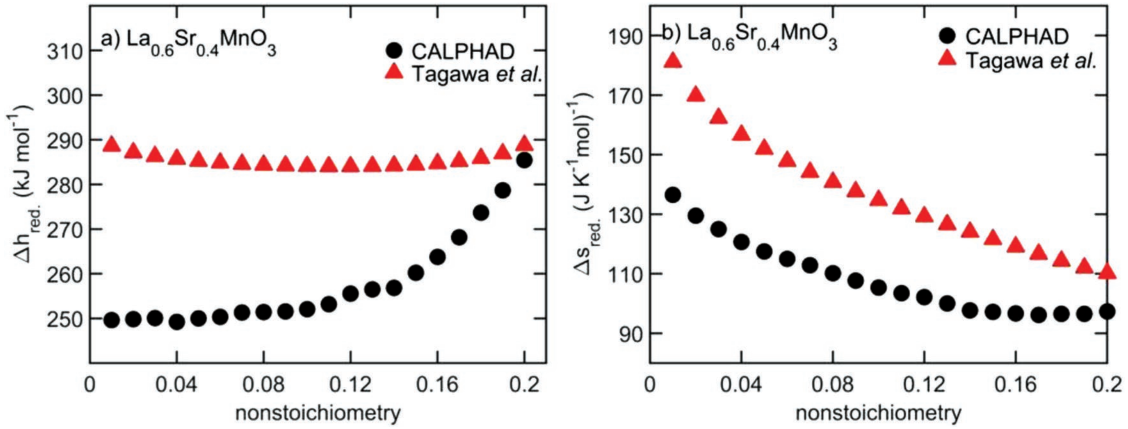

Figure 4. Thermodynamic characteristics of $La_{0.6}Sr_{0.4}MnO_{3-\delta}$ versus oxygen nonstoichiometry: a) enthalpy and b) entropy of reduction. Black dots correspond to thermodynamic properties extracted from CALPHAD data, here the red triangles represent thermodynamic entities derived from data from Tagawa et al.[26]

the compositions $La_{0.8}Sr_{0.2}MnO_{3-\delta}$, $La_{0.7}Sr_{0.3}MnO_{3-\delta}$, and $La_{0.6}Sr_{0.4}MnO_{3-\delta}$, derived from CALPHAD descriptions of oxygen nonstoichiometry **Figure** 5a–c. The effect of increasing the strontium doping on the lanthanum A-sites of the perovskite can be studied by comparing the thermodynamic quantities at an exemplary oxygen nonstoichiometry of 0.2, which is practically attainable reduction extent at typical solar-to-fuel reducing conditions. First, the enthalpy decreases with Δ15 kJ mol^{-1} from 295 to 280 kJ mol^{-1}, Figure 5a, while the entropy displays a minor increase of Δ10 J mol^{-1} K^{-1} from 85 to 95 J mol^{-1} K^{-1}, Figure 5b. Secondly, the Gibbs free energy decreases by Δ25 kJ mol^{-1} from 185 to 160 kJ mol^{-1} Figure 5c, when increasing the A-site doping strontium concentration on the perovskite`s lanthanum site. As a side remark the crystal structure of the solid solution phases $La_{1-x}Sr_xMnO_{3-\delta}$ are attributed to rhombohedral structure with a gradual transformation to orthorhombic lattice geometry with increasing x, particularly reported above $x \approx 0.25$.[47,48] Whereas the thermodynamic changes due to this transformation are not observable in the given temperature range, the associated volumetric changes during thermal cycling should be traced in the perovskite design for technological application.

We can conclude that there is substantial room to manipulate the effective oxygen vacancy concentration and exchange such as by increasing the strontium content on the lanthanum site from 0.2 to 0.4, and inflict changes in the enthalpy of 5%, entropy by 11% and Gibbs free energy of 13% at a fixed oxygen nonstoichiometry of 0.2. It is also to be noted, that if we vary the oxygen nonstoichiometry from 0.2 to 0.02, such as in a typical redox process for solar-to-fuel of water and CO_2 splitting, the enthalpy may even reduce by Δ35 kJ mol^{-1} (from 280 up to 235 kJ mol^{-1}) for $La_{0.6}Sr_{0.4}MnO_{3-\delta}$.

While the enthalpy and entropy of oxygen vacancy formation are crucial to determine the conversion ratio of water and CO_2 into chemical fuel, the heat capacity defines the solar thermal energy required to heat the reactive material between the low and high temperature step. It is therefore of high importance for the thermochemical efficiency, which we extract in the following based on the CALPHAD library for the given material compositions.

3.3. CALPHAD Heat Capacity of the Perovskite-Type Oxide $La_{1-x}Sr_xMnO_{3-\delta}$

Heat capacity values extracted from CALPHAD libraries of the compositions $La_{1-x}Sr_xMnO_{3-\delta}$ versus oxygen partial pressure and temperature are displayed in **Figure 6**. The underlying thermodynamic model parameter optimization[28,31,32,34] pertains adjustment of C, D, E, and F parameters of the molar Gibbs energy function $G_m = A + BT + CT \ln T + DT^2 + ET^3 + FT^{-1}$ for all perovskite compounds with available experimental heat capacities (typically with few components, such as $LaMnO_3$). Heat capacities of complex multicomponent perovskite are then obtained by stoichiometrically weighted sum of the heat capacities of forming compounds, i.e., without “excess” heat capacity contributions to the ideal mixture. This rough estimation, based on Neumann (1831) and Kopp’s (1864) rule that the molar heat capacity of a solid compound is the sum of the heat capacities of the elements in it, has also been chosen in the present study since experimental heat capacity data are missing in the temperature range of solar-to-fuel application. Comparison of estimated heat capacities of $LaMnO_3$ with calorimetric data from 300 up to 1073 K[35] yielded less than 8 J $mol^{-1}K^{-1}$ (≈5%) difference. This is close to experimental uncertainties and thus justifies estimation. Heat capacities are given as function of the logarithmic oxygen partial pressure range of 10^{-2}–10^{-10} and a temperature range of 1173–1873 K for the compositions $La_{0.8}Sr_{0.2}MnO_{3-\delta}$, $La_{0.7}Sr_{0.3}MnO_{3-\delta}$, and $La_{0.6}Sr_{0.4}MnO_{3-\delta}$ in Figure 6a–c respectively. Figure 6d depicts the heat capacities of $La_{1-x}Sr_xMnO_{3-\delta}$ as functions of temperature at a typical reduction oxygen partial pressure of 10^{-6} atm. Here, we observe increasing heat capacity from 150 to 170 J mol^{-1} K^{-1} in the temperature range 1173 to 1873 K, for all compositions. Literature comparison to undoped $LaMnO_3$ reveals good agreement of heat capacities determined by Jacob and Attaluri[35] for strontium doping concentrations of up to 0.3 over the classic solar-to-fuel conversion temperature range of 1173–1873 K. However, based on our CALPHAD analysis we show that this data does no longer give the most accurate description of the heat capacities at larger doping concentrations, accepting Neumann Kopp’s rule. Having established the

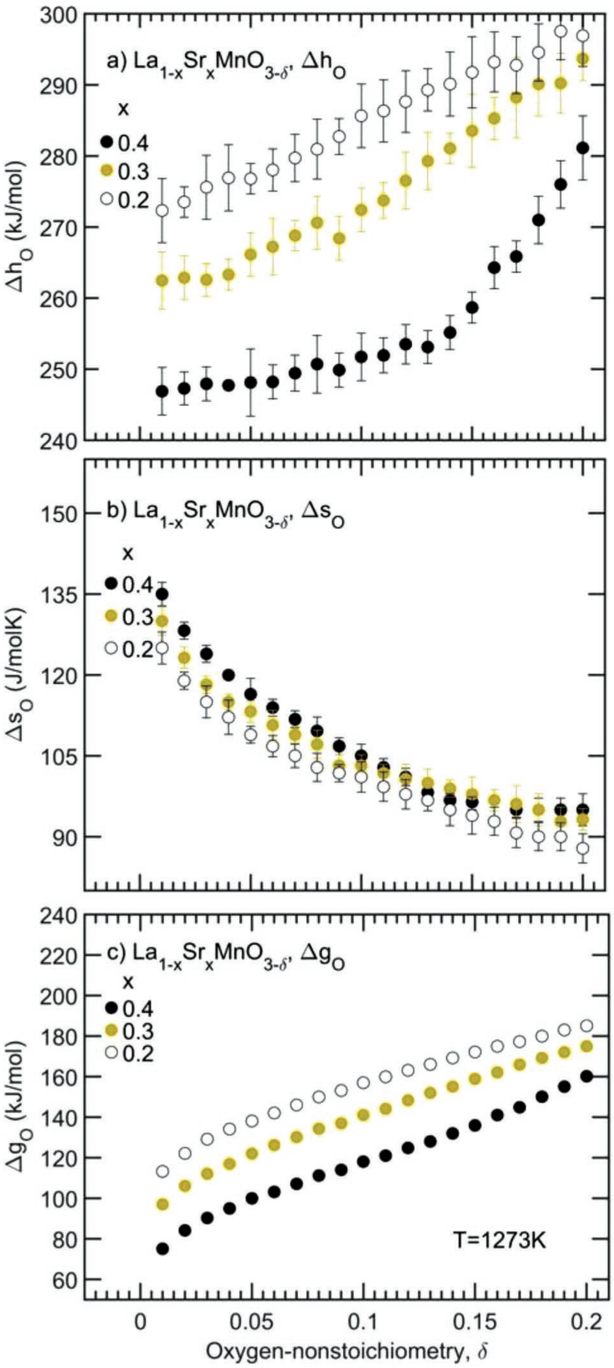

Figure 5. Thermodynamic characteristics of oxygen release of $La_{0.6}Sr_{0.4}MnO_3$, $La_{0.7}Sr_{0.3}MnO_3$, and $La_{0.8}Sr_{0.2}MnO_3$ derived from CALPHAD descriptions of defect chemistry: a) enthalpy, b) entropy, and c) Gibbs free energy change of reduction at a temperature of 1273 K as functions of oxygen nonstoichiometry.

thermodynamic properties of the perovskite materials, we turn to equilibrium models between reactant gases and the solid solutions to determine equilibrium fuel yields of the different compositions.

4. Equilibrium Thermodynamics of Thermochemical Fuel Production

Oxidation of the perovskite is thermodynamically favorable in the presence of water or CO_2 if the Gibbs free energy change of the reaction is negative. Considering for example the equilibrium thermodynamics of hydrogen production reaction in Equation (2a), it involves water splitting (Equation (5))

$$\delta H_2O(g) \leftrightarrow \delta \frac{1}{2} O_2(g) + \delta H_2(g) \tag{5}$$

with the Gibbs free energy change Δg_{H_2O} found in NIST-JANAF tables and oxidation of the perovskite, Equation (1), having a Gibbs free energy change denoted by Δg_O. For the entire water splitting reaction in Equation (2a) the standard Gibbs free energy change is given by

$$\Delta g_{ox,H_2O} = -\Delta g_O + \Delta g_{H_2O} \tag{6}$$

Provided the term $\Delta g_{ox,H_2O}$ is negative, water splitting occurs spontaneously. The thermodynamics of CO_2 splitting is qualitatively equivalent and a similar expression can be written, see Refs. [9,12,27].

If water splitting occurs spontaneously, it will proceed until an equilibrium is reached between the competing reactions of water reduction reaction (production of hydrogen) and the oxidation of the perovskite. The equilibrium hydrogen yield is thus obtained by solving the following equation iteratively[9,49]

$$\Delta g_O(\delta = \delta_i - n_{H_2}) = RT \ln\left(\frac{K_w(n_{H_2O} - n_{H_2})}{n_{H_2}}\right) \tag{7}$$

Where δ_i is the nonstoichiometry of the perovskite after reduction, n_{H_2} refers to the moles of hydrogen produced per mole metal oxide, n_{H_2O} is the water concentration, and K_w is the equilibrium constant for water splitting which is determined by Δg_{H_2O}.

4.1. Equilibrium Fuel Yields Based on CALPHAD Data Compared to Literature Results

Here, we make a quantitative comparison of our predictions based on CALPHAD data, for oxygen release and hydrogen fuel production, for the perovskite $La_{1-x}Sr_xMnO_{3-\delta}$ to results in literature. First, we proceed by making a comparison to real thermochemical cycling experiments of strontium doped lanthanum perovskites in an infrared furnace by Yang et al.,[27] **Figure 7**. Second, we compare our predictions to the calculations of equilibrium fuel yields made by Scheffe et al.[9] based on Tagawa's thermogravimetric data of oxygen nonstoichiometry in **Figure 8**.

In Figure 7, the comparison toward actual thermochemical cycling is carried out for the same conditions as in the experiment of Ref. [27], namely solar-to-fuel cycling of the reactor material between 800 and 1400 °C, with an oxygen partial pressure during reduction of 10^{-5} atm. For our calculations,

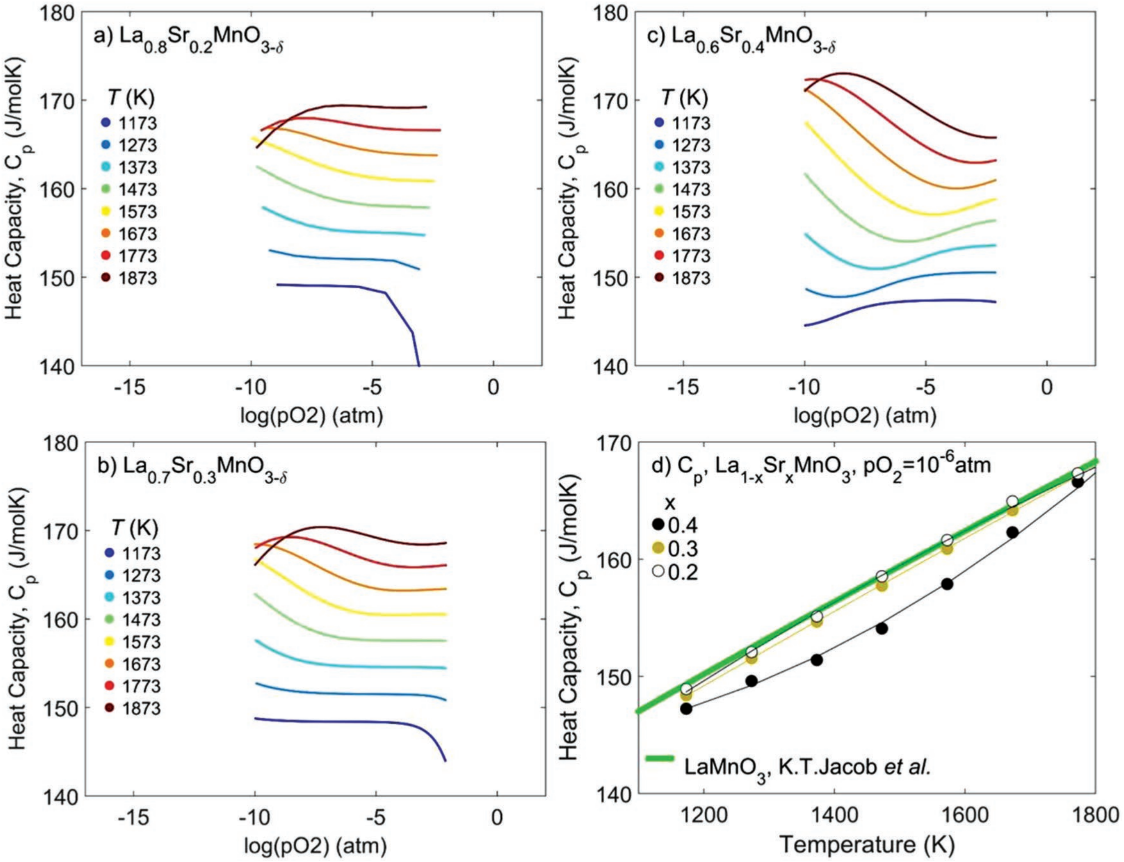

Figure 6. Heat capacity of the perovskite type oxide $La_{1-x}Sr_xMnO_{3-\delta}$ compositions extracted from CALPHAD data libraries. The heat capacity is plotted as function of logarithm oxygen partial pressure for a) $La_{0.8}Sr_{0.2}MnO_{3-\delta}$, b) $La_{0.7}Sr_{0.3}MnO_{3-\delta}$, and c) of $La_{0.6}Sr_{0.4}MnO_{3-\delta}$. d) is a plot of the heat capacity of $La_{1-x}Sr_xMnO_{3-\delta}$ as function of temperature at an oxygen partial pressure of 10^{-5} atm, compared to the heat capacity of $LaMnO_3$ given by Jacob and Attaluri.[35]

we use a water concentration of 771 per mole perovskite oxide ($n_{H_2O} = 771\ n_{ABO_3}$) during reoxidation, which is the equivalent to a water partial pressure of $p_{H_2O} = 0.2$ atm for the sample size and reactor volume given in the cited experiment, see estimation calculation in Supporting Information S1. The following trends are observed for the comparison of the CALPHAD-based predictions and experimental results relative to the strontium doping concentration of the perovskite in, Figure 7: Increasing the strontium content up to 0.4 on the A-site results in increased oxygen release and higher fuel production. Example for doping from 20 to 40 mol% strontium on the lanthanum site we compute an increase of oxygen release from 1.3 to 5.6 mL g^{-1} and elevation of the hydrogen yield from 2.6 to 8.8 mL g^{-1}.

In Figure 8, we show the equilibrium fuel yield predictions based on CALPHAD data for reduction at 1773 K, an oxygen partial pressure of 10^{-6} atm, and for two different water concentrations of 1 and 100 times the initial oxygen nonstoichiometry. These results are compared to predictions calculated by Scheffe et al.[9] for similar conditions, i.e., with a reduction temperature of 1800 K and with an oxygen partial pressure of 10^{-5} atm. For these conditions the oxygen nonstoichiometries after reduction are 0.18 in the CALPHAD based study and 0.189 in the cited study. See Figure S2 in the Supporting Information for the CALPHAD based calculation of hydrogen yields with a higher oxygen partial pressure of 10^{-5} atm and a reduction temperature of 1773 K.

For predictions based on CALPHAD data, it is observed that the equilibrium hydrogen yield increases from ≈0.07 to 0.09 moles when the temperature is decreased from 1000 to 400 K. In the cited study, the hydrogen fuel yield displays a significantly higher increase from 0.09 to 0.17 moles at water concentrations of 100 times the initial oxygen nonstoichiometry, $n_{H_2O} = 100\delta_i$. The higher fuel yields and greater increase of fuel production as function of lower temperature in the mentioned experiment can be explained by the higher estimated values of nonstoichiometry and higher values of partial molar enthalpy and entropy.

As a concluding remark, the quantitative predictions made based on CALPHAD data reproduce results on oxygen release and hydrogen yields in literature well compared to experimental results by Yang et al. for cycling between 1073 and 1673 K for the perovskites $La_{1-x}Sr_xMnO_{3-\delta}$. After re-evaluation of thermodynamic data of $La_{0.6}Sr_{0.4}MnO_{3-\delta}$ we report equilibrium fuel yield of 0.07 mole hydrogen per mole oxide compared to 0.09 in the analysis of Scheffe et al. at an oxidation temperature of 1000 K, which is related to the choice of input data. We can

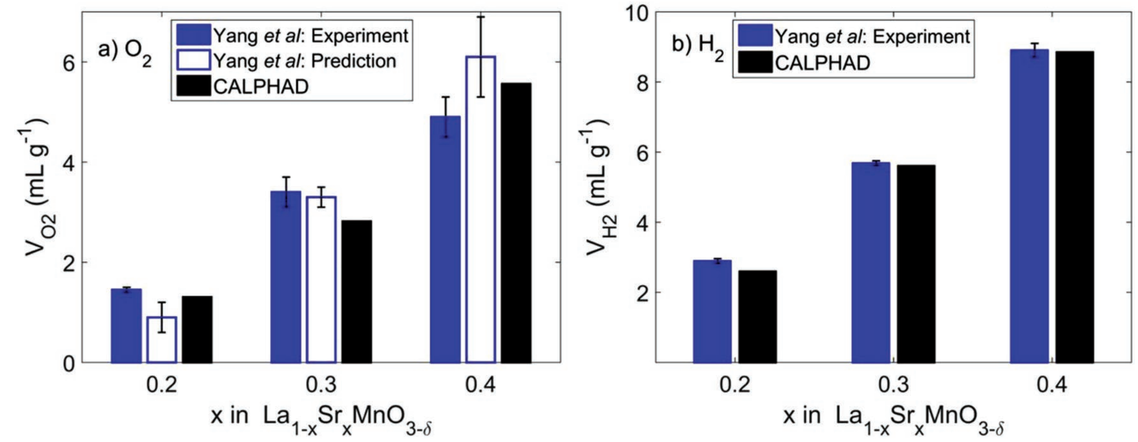

Figure 7. a) Oxygen release and b) hydrogen production for a temperature cycle of 1400–800 °C and an oxygen partial pressure during reduction of 10 ppm (10^{-5} atm). Oxygen release based on the extracted nonstoichiometry in CALPHAD at $pO_2 = 10^{-5}$ and temperature at reduction of $T_{red} = 1673$ K. Predictions of hydrogen fuel yields are based CALPHAD data with steam concentration of $n_{H_2O} = 771\ n_{ABO_3}$. In the cited experiments a water concentration of 0.2 atm H_2O in inert gas was used for all compositions, see Supporting Information of conversion 0.2 atm H_2O into moles water per mol perovskite oxide.

use the CALPHAD based analysis, to compute the variations in hydrogen yield and oxygen release and find that increasing the strontium content from 0.2 to 0.4 on the A-site, results in an increase in hydrogen yield from 2.6 to 8.8 mL g^{-1} for a high water concentration. We highlight that a comparison of fuel productivity is beneficial to determine the feasibility of solar-to-fuel material, but it cannot stand alone as an assessment of performance, since it is highly dependent on the water concentration. Here, it is vital to consider all energies required to produce that fuel, e.g., heat required to heat the steam and sensible heat of the metal oxide, which encourages determination of the thermochemical solar-to-fuel conversion efficiency, which will be determined in the following.

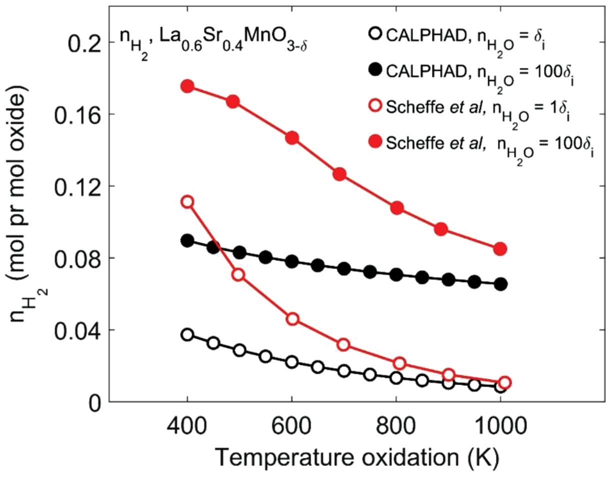

Figure 8. Equilibrium hydrogen yield of the perovskite $La_{0.6}Sr_{0.4}MnO_{3-\delta}$ for two different water concentrations of $n_{H_2O} = 1\ \delta_i$ and $n_{H_2O} = 100\ \delta_i$ as function of oxidation temperature. Reduction is carried out at a temperature of 1773 K and an oxygen partial pressure is $pO_2 = 10^{-6}$ atm (initial nonstoichiometry is 0.18 for these conditions). Equilibrium fuel yields are calculated based on oxygen nonstoichiometry and heat capacity from CALPHAD data libraries and compared to the results obtained by Scheffe et al.[9] for the same composition at 1800 K and $pO_2 = 10^{-5}$ atm (initial nonstoichiometry is 0.189).

5. Efficiency Analysis

Thermochemical solar-to-fuel efficiency, $\eta_{\text{solar-to-fuel}}$, is defined by the useful output energy divided by the input energy

$$\eta_{\text{solar-to-fuel}} = \frac{\mathrm{HHV}_{H_2} n_{H_2}}{Q_{\text{solar}} + E_{\text{penalties}}} \tag{8}$$

Here, the useful energy is simply the fuel yield, n_{H_2}, multiplied by the higher heating value of hydrogen, HHV_{H_2}. The input energy is the sum of Q_{solar} and $E_{\text{penalities}}$, where the latter is the reactor specific losses. The term $E_{\text{penalities}}$ is dependent on reactor type and method of operation and will be set to zero, because focus of this analysis is on the relative performance of each material. The solar input, Q_{solar}, is given by

$$Q_{\text{solar}} = \frac{1}{\eta_{\text{abs}}}\left(\Delta h_{H_2O|_{298\,K \to T_{ox}}} n_{H_2O,i} + \int_{T_{ox}}^{T_{red}} c_p \, dT + \Delta h_{red} \delta n_{ox}\right) \tag{9}$$

The first term $\Delta h_{H_2O|_{298\,K \to T_{ox}}}$ is the energy required to heat water from room temperature to the water splitting temperature T_{ox}. The second term including c_p is the heat capacity of the reactive material, and the latter term, Δh_{red}, is the enthalpy change in the temperature window from the oxidation temperature to the reduction temperature for each cycle

$$\Delta h_{red} = \frac{\int_{\delta_i}^{\delta_f} \Delta h_O \, d\delta}{\delta_i - \delta_f} \tag{10}$$

Here, Δh_O is the enthalpy of reduction found via Equation (4). δ_i is the oxygen nonstoichiometry after reduction at the high temperature step, and δ_f is the nonstoichiometry after reoxidation by water at the low temperature step. The solar absorption efficiency in Equation (9) for a blackbody receiver is given by the following in accordance to Ref. [2]

$$\eta_{abs} = 1 - \frac{\sigma T^4}{IC} \tag{11}$$

Here σ is the Stefan–Boltzmann constant, I is direct normal irradiation ($I = 1$ kW m^{-2} in this work) and $C = 5000$ is the solar flux concentration ratio.

5.1. Comparison of Thermochemical Solar-to-fuel Efficiency of $La_{0.6}Sr_{0.4}MnO_{3-\delta}$ Based on CALPHAD Data to Thermogravimetric Input Data

In **Figure 9**, thermochemical solar-to-fuel efficiency obtained by analysis of heat capacity and oxygen nonstoichiometry data extracted from CALPHAD libraries are plotted and compared to the results obtained by Scheffe et al.,[9] using input data from Ref. [26] and heat capacity of $LaMnO_3$ from Ref. [35], exemplified by the perovskite $La_{0.6}Sr_{0.4}MnO_3$. The conditions during reduction in the CALPHAD based calculation is chosen to match the oxygen nonstoichiometry in work from Scheffe et al.[9] after reduction to enable comparison of the thermodynamic properties governing the splitting reaction. The efficiency is plotted as function of oxidation temperature in the range 400–1000 K for two different steam concentrations, namely, 1 and 100 times the initial nonstoichiometry, and it is noted that the energy required to heat excess steam is not included in either analysis.

The CALPHAD efficiency is generally lower than the cited efficiency. For the high water concentration (100 δ_i), the CALPHAD efficiency decreases from 12% to 10% as function of temperature, whereas Scheffe et al. predicts an efficiency increase from 14% to 17%. The lower efficiency is explained by lower equilibrium fuel yields, which is further related to lower values of oxygen nonstoichiometry and lower absolute values of the thermodynamic functions. We assign more weight to the CALPHAD data, since it is given in the relevant temperature range of 1073–1873 K, while the input data for the cited analysis covers a narrower range of 873–1273 K. Having studied the thermochemical solar-to-fuel efficiency of the perovskite $La_{0.6}Sr_{0.4}MnO_{3-\delta}$ it is clear that increased water concentration enhances the efficiency, but effective recuperation of excess steam is necessary to achieve those efficiencies. Further, it is evident that the choice of input data on oxygen nonstoichiometry and heat capacity is crucial. Using CALPHAD data, results in lower efficiency, compared to data used in previous analysis due to lower oxygen nonstoichiometry. Even though thermochemical water splitting becomes increasingly thermodynamically favorable at lower temperatures, the energy penalty of increased swing in temperature is greater than the gain in fuel production. We now turn the effect of varying strontium contents in $La_{1-x}Sr_xMnO_{3-\delta}$ and the implications of diverse reactor operation schemes.

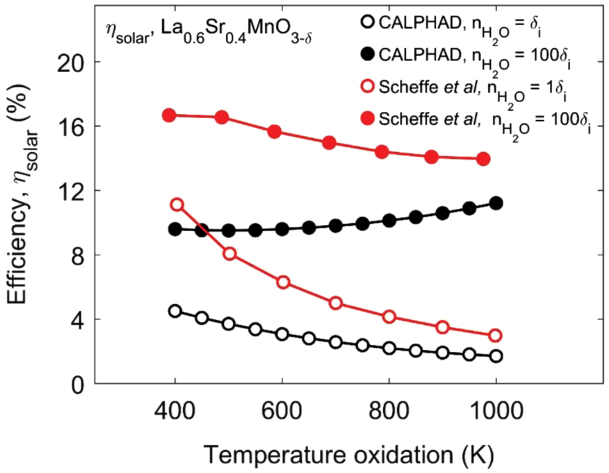

Figure 9. Solar thermochemical fuel efficiency of $La_{0.6}Sr_{0.4}MnO_{3-\delta}$ as function of oxidation temperature for two different water concentrations of $n_{H_2O} = 1\ \delta_i$ and $n_{H_2O} = 100\ \delta_i$. Reduction temperature is 1773 K, oxygen partial pressure is $pO_2 = 10^{-6}$ atm ($\delta_i = 0.18$). Calculations of efficiency are based on oxygen nonstoichiometry and heat capacity from CALPHAD data libraries and compared to the results obtained by Scheffe et al.[9] for the same composition at 1773 K and $pO_2 = 10^{-5}$ atm ($\delta_i = 0.189$).

5.2. Solar Thermochemical Fuel Efficiency of $La_{1-x}Sr_xMnO_{3-\delta}$ Based on CALPHAD Data

In **Figure 10**, the equilibrium hydrogen yield and the solar thermochemical fuel efficiency is plotted for different reaction conditions, such as temperature swing settings (i.e., oxidation and reduction temperature) and water concentration, and we investigate how this affects the performance of different perovskite compositions $La_{1-x}Sr_xMnO_{3-\delta}$ with $x = 0.2$, 0.3, and 0.4:

The effect of different water concentration, n_{H_2O}, is studied in Figure 10a,b for a temperature cycle of 1473–1773 K, and an oxygen partial pressure during reduction of 10^{-6} atm: For a water concentration equal to the initial oxygen nonstoichiometry (i.e., $n_{H_2O} = \delta_i$) the efficiency is in the range 1%–1.5%, with the highest efficiency given for the composition $La_{0.6}Sr_{0.4}MnO_{3-\delta}$. Increasing the water concentration by a factor of 100 (i.e., $n_{H_2O} = 100\delta_i$) the efficiency increases to 17.5%, 19%, and 18.5% for the compositions $La_{0.6}Sr_{0.4}MnO_{3-\delta}$, $La_{0.7}Sr_{0.3}MnO_{3-\delta}$, and $La_{0.8}Sr_{0.2}MnO_{3-\delta}$, respectively. Hence, the composition $La_{0.7}Sr_{0.3}MnO_{3-\delta}$ has the highest efficiency despite having a lower fuel production than $La_{0.6}Sr_{0.4}MnO_{3-\delta}$ at $n_{H_2O} = 100\delta_i$.

We elucidate the importance of oxidation temperatures, 1073–1773 K, for a fixed reduction temperature of 1773 K, $n_{H_2O} = 10\ \delta_i$, and a reduction partial pressure of 10^{-6} atm, in Figure 10c,d. At an oxidation temperature of 1073 K, the composition with 30 mol% strontium, has a slightly higher efficiency of 6.8% compared to 6.2% and 5.8% for the compositions with 20 and 40 mol%. Interestingly, we observe that a smaller difference between reduction and oxidation temperature increases efficiency. For isothermal cycling at 1773 K and moderate water concentration of $n_{H_2O} = 10\ \delta_i$, the efficiency reaches a maximum value of 21% for the composition $La_{0.8}Sr_{0.2}MnO_{3-\delta}$. Increasing strontium content at these conditions, results in a decrease in efficiency to

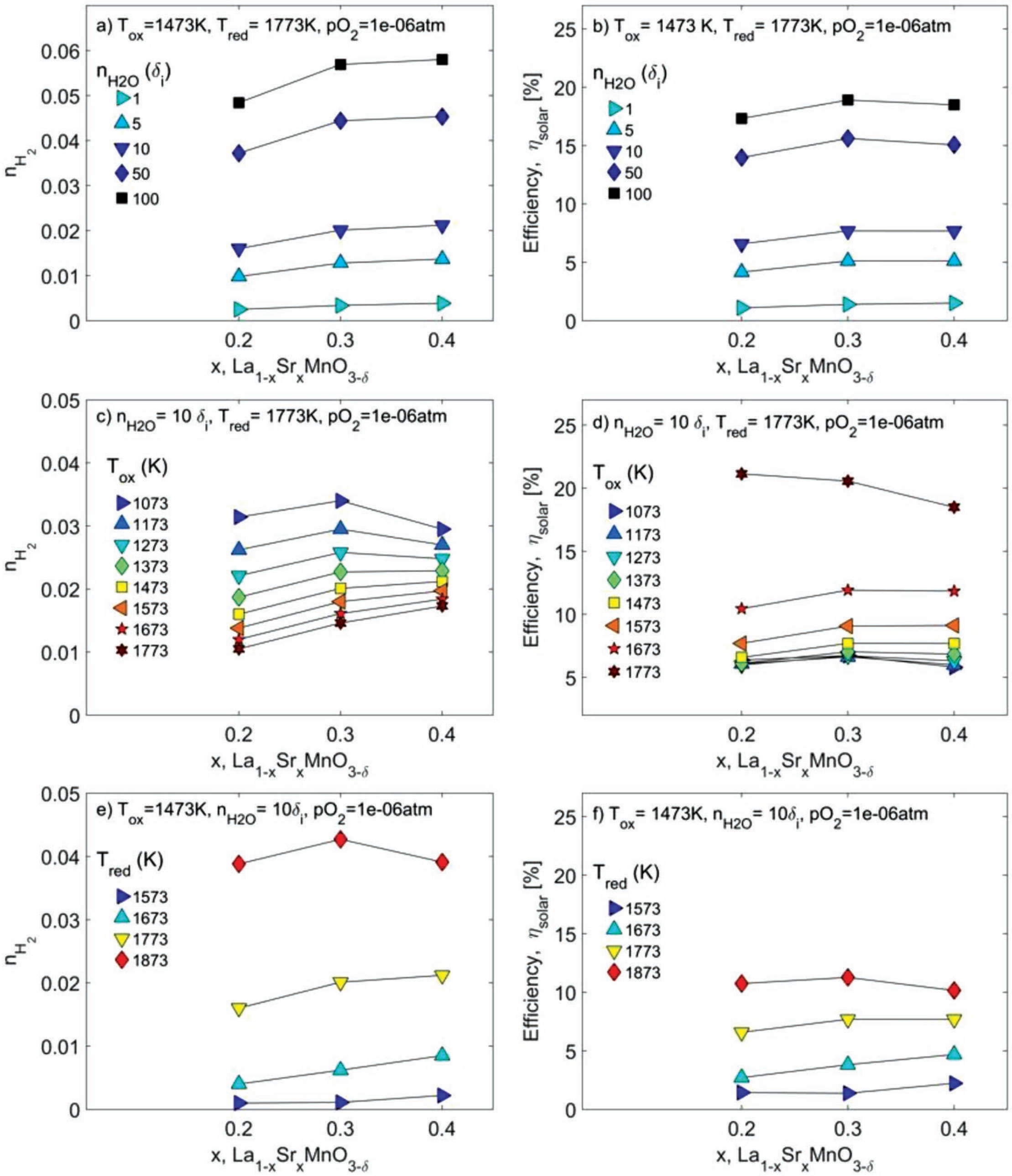

Figure 10. Predicted equilibrium hydrogen yields and thermochemical efficiency of $La_{0.8}Sr_{0.2}MnO_{3-\delta}$, $La_{0.7}Sr_{0.3}MnO_{3-\delta}$, and $La_{0.6}Sr_{0.4}MnO_{3-\delta}$ for different reactor temperatures and steam concentrations. Energy to heat excess steam is not included in the calculation of efficiency. Effect of steam concentration, n_{H_2O} with oxidation at 1473 K and reduction at 1773 K in (a,b). Followed by effect of oxidation temperature, T_{ox}, for reduction at 1773 K and a steam concentration of $n_{H_2O} = 10\ \delta_i$ in (c,d). Finally, the effect of reduction temperature is shown in (e,f) for oxidation at a temperature of 1473 K and a water concentration of $n_{H_2O} = 10\delta_i$. In all experiments, the oxygen partial pressure during reduction is 10^{-6} atm.

20.5% and 18.5% for the compositions $La_{0.7}Sr_{0.3}MnO_{3-\delta}$ and $La_{0.6}Sr_{0.4}MnO_{3-\delta}$ respectively.

The influence of reduction temperature in the range 1573–1873 K is shown in Figure 10e,f for an oxidation temperature of 1473 K, an oxygen partial pressure during reduction of 10^{-6} atm and $n_{H_2O} = 10\ \delta_i$. From our predictions based on CALPHAD data, it is observed that increasing the strontium doping from 20 to 40 mol% on the A-site increases the efficiency in the temperature range 1573–1673 K. For a higher reduction temperature this dependence on strontium changes and the composition $La_{0.7}Sr_{0.3}MnO_{3-\delta}$ has the highest efficiency of 7.5% and 11.2% at the temperatures 1773 and 1873 K respectively.

To summarize, the strontium content on the A-site of $La_{1-x}Sr_xMnO_{3-\delta}$ plays a major role for fuel yields and the thermochemical solar-to-fuel efficiency. In most cases, the composition $La_{0.6}Sr_{0.4}MnO_{3-\delta}$ has the highest fuel production; but it is surpassed in efficiency by the compositions with a lower doping mole% of strontium. Example, the composition

$La_{0.7}Sr_{0.3}MnO_{3-\delta}$ has the highest efficiency of 19% for reduction at 1773 K and oxidation at 1473 K even though it displays lower fuel production than $La_{0.6}Sr_{0.4}MnO_{3-\delta}$ at the given conditions. The composition $La_{0.7}Sr_{0.3}MnO_{3-\delta}$ displays high efficiencies due to having considerable oxygen release at moderate temperature balanced by favorable thermodynamics for water splitting. For reference, the target efficiency in the solar-to-fuel field is typically set at 20% to offer a competitive alternative to existing technologies.[8] It is exceeded by the composition $La_{0.8}Sr_{0.2}MnO_{3-\delta}$ with an efficiency of 21% for isothermal water splitting at 1773 K, offering an intriguing alternative to two-step thermochemical solar-to-fuel production. Also, $La_{0.8}Sr_{0.2}MnO_{3-\delta}$ will be less prone to structural change during thermal cycling compared to compositions with more strontium.

Further, we remark that the equilibrium fuel yields of all tested perovskite compositions increase for lower oxidation temperature because the entropy term in $\Delta g_{\mathrm{ox,H_2O}}$ in Equation (6) is positive. However, the overall efficiency decreases for lower oxidation temperature, because the entropy term is small, Figure 9c,d. Due to the small entropy, the thermodynamic driving force for water splitting increases slightly, but the gain in produced fuel is outweighed by increase in energy penalty of increased temperature swing. For comparison the partial molar entropy of the perovskite $La_{0.8}Sr_{0.2}MnO_{3-\delta}$ is $\Delta s_O = 105$ J mol^{-1} K^{-1} at an oxygen-nonstoichiometry of 0.1, while ceria has an entropy of $\Delta s_O = 220$ J mol^{-1} K^{-1}[24] making the perovskite more viable for isothermal thermochemical fuel production. Here, it has to be considered that the fuel yields during isothermal water splitting are low and the relative influence of reactor specific losses will be larger for the efficiency.

6. Conclusions

In this work, we demonstrate a full analysis of equilibrium fuel yields and solar-to-fuel efficiency of the perovskite $La_{1-x}Sr_xMnO_{3-\delta}$ within the concentration range of 20–40 mol% strontium on the A-site. We selected the present perovskite material as a model case to demonstrate on the one hand the usefulness of existing CALPHAD libraries on oxygen nonstoichiometry and heat capacity in the entire temperature range of 1073–1873 K relevant for solar-to-fuel conversion as input data for all calculations, and to allow a direct comparison to experimental and computational data in literature.

The strontium doping level on the A-site is of high importance for the equilibrium fuel production as well as thermochemical efficiency and it is strongly dependent on reaction conditions, such as steam concentration and operation temperature. For very high steam concentrations, ($n_{H_2O} = 771\ n_{ABO_3}$) and cycling between 800 and 1400 °C the CALPHAD based calculations show increased fuel production with increased strontium doping level with a maximum of 8.8 mL g^{-1} for the compositions $La_{0.6}Sr_{0.4}MnO_{3-\delta}$. For more moderate water concentrations ($n_{H_2O} < 100\ \delta_i$) the composition with highest strontium content, i.e., $La_{0.6}Sr_{0.4}MnO_{3-\delta}$, has the highest fuel yield in many cases, but it does not have the highest efficiency. Here, the material with intermediate strontium doping level, $x = 0.3$, displays the highest efficiency with a maximum of 19% for thermal reduction at 1773 K and reoxidation at 1473 K for $n_{H_2O} = 10\ \delta_i$. This particular composition displays a tradeoff between considerable oxygen release and favorable thermodynamics for water splitting. Interestingly, we report that the perovskite $La_{0.8}Sr_{0.2}MnO_{3-\delta}$ has the maximum efficiency of 21% for isothermal thermochemical cycling at 1773 K and a water concentration of only $n_{H_2O} = 10\ \delta_i$.

The given perovskite shows promise to thermochemical due to efficiencies higher than the solar-to-fuel target efficiency of 20% to be commercially competitive. In this context, it should be noted that the obtained efficiencies are calculated without accounting the energy penalty of heating excess steam, which lowers the efficiency. Further, it was shown that the choice of input data for the calculations plays a significant role for predictions of fuel yields and thermochemical efficiency. Our calculations based on CALPHAD data determined in the actual operating temperature range, display 22% and 14% lower fuel production and efficiency respectively for similar conditions as earlier studies. The discrepancy arises from choice of input data and overestimates of extrapolated oxygen nonstoichiometry values in previous works.

The versatility of perovskites for incorporating numerous different elements on both cationic sites and alter the thermodynamic properties holds promise to the discovery of new efficient materials for solar-to-fuel conversion. The benefits of applying the comprehensive CALPHAD approach to describe perovskites is in part because of the reliability of the descriptions of the thermodynamic properties as well as the opportunity to predict the properties of complex multicomponent perovskites by including other A- and B-site cations and predict new efficient materials. These descriptions are not only relevant to the solar-to-fuel field but in other research areas where the thermodynamic parameters define the material performance such as thermal energy storage, chemical looping combustion, and metal oxides catalyzing the production of methane.

Supporting Information

Supporting Information is available from the Wiley Online Library or from the author.

Acknowledgements

The authors acknowledge financial support by the ETH Foundation for this work, grant number ETH-05 13-1.

Received: May 24, 2016
Revised: July 20, 2016

---

[1] W. C. Chueh, C. Falter, M. Abbott, D. Scipio, P. Furler, S. M. Haile, A. Steinfeld, *Science* **2010**, *330*, 1797.
[2] A. Steinfeld, *Solar Energy* **2005**, *78*, 603.
[3] A. H. McDaniel, E. C. Miller, D. Arifin, A. Ambrosini, E. N. Coker, R. O'Hayre, W. C. Chueh, J. Tong, *Energy Environ. Sci.* **2013**, *6*, 2424.
[4] S. Dey, B. S. Naidu, A Govindaraj, C. N. R. Rao, *Phys. Chem. Chem. Phys.* **2015**, *17*, 122.

[5] A. Bork, M. Kubicek, M. Struzik, J. L. M. Rupp, *J. Mater. Chem. A* **2015**, *3*, 15546.
[6] T. Cooper, J. R. Scheffe, M. E. Galvez, R. Jacot, G. Patzke, A. Steinfeld, *Energy Technol.* **2015**, *3*, 1130.
[7] M. Takacs, M. Hoes, M. Caduff, T. Cooper, J. R. Scheffe, A. Steinfeld, *Acta Mater.* **2016**, *103*, 700.
[8] N. P. Siegel, J. E. Miller, I. Ermanoski, R. B. Diver, E. B. Stechel, *Ind. Eng. Chem. Res.* **2013**, *52*, 3276.
[9] J. R. Scheffe, D. Weibel, A. Steinfeld, *Energy Fuels* **2013**, *27*, 4250.
[10] J. E. Miller, A. H. McDaniel, M. D. Allendorf, *Adv. Energy Mater.* **2014**, *4*, 1300469.
[11] D. Marxer, P. Furler, J. Scheffe, H. Geerlings, C. Falter, V. Batteiger, A. Sizmann, A. Steinfeld, *Energy Fuels* **2015**, *29*, 3241.
[12] M. Takacs, J. Scheffe, A. Steinfeld, *Phys. Chem. Chem. Phys.* **2015**, *17*, 7813.
[13] S. Ackermann, L. Sauvin, R. Castiglioni, J. L. M. Rupp, J. R. Scheffe, A. Steinfeld, *J. Phys. Chem. C* **2015**, *119*, 16452.
[14] M. Zinkevich, D. Djurovic, F. Aldinger, *Solid State Ionics* **2006**, *177*, 989.
[15] M. Mogensen, N. M. Sammes, G. A. Tompsett, *Solid State Ionics* **2000**, *129*, 63.
[16] J. L. M. Rupp, E. Fabbri, D. Marrocchelli, J.-W. Han, D. Chen, E. Traversa, H. L. Tuller, B. Yildiz, *Adv. Functional Mater.* **2014**, *24*, 1562.
[17] Y. Shi, A. H. Bork, S. Schweiger, J. L. M. Rupp, *Nat. Mater.* **2015**, *14*, 721.
[18] A. O. Stoermer, J. L. Rupp, L. J. Gauckler, *Solid State Ionics* **2006**, *177*, 2075.
[19] M. Kuhn, S. R. Bishop, J. L. M. Rupp, H. L. Tuller, *Acta Mater.* **2013**, *61*, 4277.
[20] N. Yang, Y. Shi, S. Schweiger, E. Strelcov, A. Belianinov, V. Foglietti, P. Orgiani, G. Balestrino, S. V. Kalinin, J. L. M. Rupp, *ACS Appl. Mater. Interfaces* **2016**, *8*, 14613.
[21] I. Ermanoski, J. Miller, M. Allendorf, *Phys. Chem. Chem. Phys.* **2014**, *16*, 8418.
[22] I. Ermanoski, N. P. Siegel, E. B. Stechel, *J. Solar Energy Eng.* **2013**, *135*, 031002.
[23] C. Jarrett, W. Chueh, C. Yuan, Y. Kawajiri, K. H. Sandhage, A. Henry, *Solar Energy* **2016**, *123*, 57.
[24] R. Panlener, R. Blumenthal, J. Garnier, *J. Phys. Chem. Solids* **1975**, *36*, 1213.
[25] M. A. Panhans, R. Blumenthal, *Solid State Ionics* **1993**, *60*, 279.
[26] H. Tagawa, N. Mori, H. Takai, Y. Yonemura, H. Minamiue, H. Inaba, T. Hashimoto, Achen, Germany, in *Proc. of 5th Int. Sympos. Solid Oxide Fuel Cells (SOFC-V)*. **1997**, June 2-5, 785.
[27] C.-K. Yang, Y. Yamazaki, A. Aydin, S. M. Haile, *J. Mater. Chem. A* **2014**, *2*, 13612.
[28] A. N. Grundy, B. Hallstedt, L. J. Gauckler, *Calphad* **2004**, *28*, 191.
[29] M. Oishi, K. Yashiro, K. Sato, J. Mizusaki, T. Kawada, *J. Solid State Chem.* **2008**, *181*, 3177.
[30] H. L. Lukas, S. G. Fries, B. Sundman, *Computational Thermodynamics: The Calphad Method*, Vol. *131*, Cambridge University Press, Cambridge **2007**.
[31] A. N. Grundy, M. Chen, L. J. Gauckler, B. Hallstedt, *J. Phase Equilib. Diffus.* **2005**, *26*, 131.
[32] A. N. Grundy, E. Povoden-Karadeniz, T. Ivas, L. J. Gauckler, *Calphad* **2006**, *30*, 33.
[33] E. Povoden-Karadeniz, M. Chen, A. N. Grundy, T. Ivas, L. J. Guackler, *J. Phase Equilib. Diffus.* **2009**, *30*, 12.
[34] E. Povoden-Karadeniz, M. Chen, T. Ivas, A. N. Guackler, *J. Mater. Res.* **2012**, *27*, 1915.
[35] K. Jacob, M. Attaluri, *J. Mater. Chem.* **2003**, *13*, 934.
[36] I. Dincer, M. Rosen, *Thermal Energy Storage: Systems and Applications*, John Wiley & Sons, The Atrium, Southern Gate, Chichester, West Sussex, United Kingdom, **2002**.
[37] A. J. Carrillo, D. Sastre, D. P. Serrano, P. Pizarro, J. M. Coronado, *Phys. Chem. Chem. Phys.* **2016**, *18*, 8039.
[38] Q. Imtiaz, D. Hosseini, C. R. Müller, *Energy Technol.* **2013**, *1*, 633.
[39] Q. Imtiaz, A. Kurlov, J. L. M. Rupp, C. R. Muller, *ChemSusChem* **2015**, *8*, 2055.
[40] W. C. Chueh, S. M. Haile, *ChemSusChem* **2009**, *2*, 735.
[41] S. Dey, B. Naidu, C. Rao, *Chem. Eur. J.* **2015**, *21*, 7077.
[42] A. N. Grundy, B. Hallstedt, L. J. Gauckler, *J. Phase Equilib. Diffus.* **2004**, *25*, 311.
[43] A. N. Grundy, B. Hallstedt, L. J. Gauckler, *Acta Mater.* **2002**, *50*, 2209.
[44] A. N. Grundy, *CALPHAD Assessment of the La-Sr-Mn-O System and the Defect Chemistry of (La, Sr) MnO$_3$ Perovskites Used as Solid Oxide Fuel Cell Cathode Materials*, ETH Zurich, Zurich **2004**.
[45] L. Rørmark, S. Stolen, K. Wiik, T. Grande, *J. Solid State Chem.* **2002**, *163*, 186.
[46] C. Laberty, A. Navrotsky, C. N. R. Rao, P. Alphonse, *J. Solid State Chem.* **1999**, *145*, 77.
[47] K. McBride, J. Cook, S. Gray, S. Felton, L. Stella, D. Poulidi, *CrystEngComm* **2016**, *18*, 407.
[48] C. Paiva-Santos, R. F. C. Marques, M. Jafelicci, L. C. Varanda, *Powder Diffr.* **2002**, *17*, 149.
[49] J. R. Scheffe, A. Steinfeld, *Energy Fuels* **2012**, *26*, 1928.